

bradscholars

Optimisation of design and operating parameters of reverse osmosis process for the removal of phenol from wastewater

Item Type	Article
Authors	Khan, Shamraze;Al-Obaidi, Mudhar A.A.R.;Kara-Zaitri, Chakib;Mujtaba, Iqbal
Citation	Khan S, Al-Obaidi M, Kara-Zaitri et al (2023) Optimisation of design and operating parameters of reverse osmosis process for the removal of phenol from wastewater. South African Journal of Chemical Engineering. 43: 79-90.
DOI	https://doi.org/10.1016/j.sajce.2022.10.005
Rights	© 2022 The Author(s). Published by Elsevier B.V. on behalf of Institution of Chemical Engineers. All rights reserved. Reproduced in accordance with the publisher's self-archiving policy. This manuscript version is made available under the CC-BY-NC-ND license (https://creativecommons.org/licenses/by-nc-nd/4.0/)
Download date	2026-04-12 09:36:35
Link to Item	http://hdl.handle.net/10454/19191



Optimisation of design and operating parameters of reverse osmosis process for the removal of phenol from wastewater[☆]

Shamraze Khan^a, Mudhar A. Al-Obaidi^{b,c}, C. Kara-Zaitri^a, I.M. Mujtaba^{a,*}

^a Department of Chemical Engineering, Faculty of Engineering and Informatics, University of Bradford, Bradford, West Yorkshire BD7 1DP, United Kingdom

^b Middle Technical University, Technical Institute of Baquba, Baquba, Dayala, Iraq

^c Middle Technical University, Technical Instructor Training Institute, Baghdad, Iraq

ARTICLE INFO

Keywords:

Wastewater treatment
Reverse osmosis
Phenol
Simulation
Modelling

ABSTRACT

Reverse Osmosis (RO) is widely used for separating organic and inorganic pollutants in wastewater. In this research, the one-dimensional steady state model of a spiral wound RO for the removal of phenol from wastewater, was simulated using gPROMS software to identify optimal design and operating parameters. The design parameters included the membrane length, width and feed spacer channel and operating conditions included temperature and pressure of the RO process. The optimal design parameters were able to maximise the removal of phenol from wastewater. The simulation results showed that the removal of phenol from wastewater was significantly influenced by the combination of membrane width, operating pressure, and feed temperature. The four main parameters (permeate concentration, solute flow, solute rejection, and water flux) that govern the performance of a reverse osmosis membrane were found to be influenced by the design and operating conditions.

1. Introduction

The ever-increasing population and associated industrialisation have contributed to a significant increase in the amount of industrial waste, including more specifically large volumes of wastewater of varying quantity and harmfulness (Zhang et al., 2020). The urgent need for water recycling and wastewater treatment has never been greater than today. Due to the exponential increase in water demand, low-quality water is often re-used in cooling towers and power plants (Pan et al., 2018). Current research shows a significant interest in recycling, recovering and reusing a variety of wastewater. Even in water rich countries, people are exploring water reuse, and are using every effort to reduce the volume of wastewater discharged into surface water, thus preserving a green environment (Tortajada, 2020). A significant volume of research is focused on removing micro-pollutants from wastewater because of their detrimental effect on both the natural environment and human health. This is no trivial task, as the removal of such organic contaminants present in wastewater is both difficult and costly (Zheng et al., 2013).

A variety of organic and non-organic chemical substances can readily be found in wastewater as a result of complicated technologies and products used in various industries (Chaturvedi, 2022; Al-Obaidi et al.,

2018). Such harmful substances are then discharged into a wide range of water resources, they disturb the whole ecosystem and have a significant impact on rivers and lakes which are used for drinking water (Liang et al., 2020). There is therefore an urgent and ever increasing need to ensure that such toxic substances are not released into the environment, and are closely controlled.

Despite the existence of physicochemical, biological and advanced treatment methods of wastewater such as adsorption, coagulation-flocculation, activated sludge, ion exchange, and oxidation processes (Mohammadi et al., 2015), Reverse Osmosis process (RO) is by far, the leading treatment technique for wastewater treatment (Al-Obaidi et al., 2020a). In an RO process, a semi-permeable membrane is used to isolate two mediums of varying solution concentration. This has been successfully used for extracting harmful contaminants from seawater and wastewater by injecting the solution at a higher pressure than the osmotic pressure inside a closed vessel (Attarde et al., 2017).

RO membrane modules are available in a variety of configurations and are used in many different applications. Specifically, the spiral wound membrane is one of the most well-known RO modules. It provides a higher packing density and a lower operating cost than conventional membranes. It comprises of a flat sheet membrane sandwich and spacers wrapped in a central permeate channel. The feed solution flows axially through the sandwich in the spacer channel. The

[☆] VSI: Sustainable Development

* Corresponding author.

E-mail address: I.M.Mujtaba@bradford.ac.uk (I.M. Mujtaba).

Nomenclature	
Symbols	
B	Feed channels friction parameter, (atm s/m ⁴)
B _s	The solute permeability coefficients of the membrane, (the Solution-diffusion model) (m/s)
c ₁ , c ₂	Constants in Eq. (33)
C _{m(x)}	Dimensionless solute concentration at any point along the membrane length
C _s	Brine solute concentration in the feed channel, (kmol/m ³)
C _{s(av)}	The mean solute concentration in the feed side, (kmol/m ³)
C _{p(av)}	Average permeate solute concentration in the permeate channel, (kmol/m ³)
C _{w(x)}	Solute concentration at the membrane wall at any point along the membrane length, (kmol/m ³)
D _{b(x)}	Diffusivity coefficient of feed at any point along the membrane length, (m ² /s)
D _{p(x)}	Diffusivity coefficient of permeate at any point along the membrane length, (m ² /s)
F _{b(x)}	Feed flow rate at any point along the membrane length, (m ³ /s)
F _{p(x)}	Permeate flow rate at any point along the membrane length, (m ³ /s)
F _{p(Total)}	Total permeated flow rate at the permeate channel, (m ³ /s)
J _{s(x)}	Solute molar flux through the membrane at any point along the membrane length, (kmol/m ² s)
J _{w(x)}	Water flux at any point along the membrane length, (m/s)
k _(x)	Mass transfer coefficient at any point along the membrane length, (m/s)
Length of the membrane, (m)	
L _p	Solvent transport coefficient, (m/atm s)
P _{b(x)}	Feed channel pressure at any point along the membrane length, (atm)
P _p	Permeate channel pressure, (atm)
R	Gas law constant, (R = 0.082 $\frac{\text{atm} \cdot \text{m}^3}{\text{K} \cdot \text{kmol}}$)
r	Parameter defined in Eq. (18)
Re _{f(x)}	The feed Reynolds number at any point along the membrane length (dimensionless)
Re _{j(av)}	Solute rejection coefficient, (dimensionless)
Re _{p(x)}	The permeate Reynolds number at any point along the membrane length (dimensionless)
Sc _{f(x)}	The feed Schmidt number at any point along the membrane length (dimensionless)
Sc _{p(x)}	The permeate Schmidt number at any point along the membrane length (dimensionless)
Sh _(x)	Sherwood number at any point along the membrane length (dimensionless)
SSE	The sum of square errors
T _b	Feed temperature, (°C)
t _f	Feed spacer thickness, (m)
W	Width of the membrane, (m)
x	Any point along the membrane length
Z	Parameter defined in Eq. (17)
Subscript	
ρ _{f(x)}	Feed density at each point along the membrane length, (kg/m ³)
ρ _m	The molal density of water, (55.56 kmol/m ³)
ρ _{p(x)}	Feed density at each point along the membrane length, (kg/m ³)
μ _{f(x)}	Feed viscosity at each point along the membrane length, (kg/m s)
μ _{p(x)}	Feed viscosity at each point along the membrane length, (kg/m s)
σ	The reflection coefficient, (dimensionless)
ω	The solute permeability coefficients of the membrane (kmol/m ² s atm)
Δx	Length of the sub-section, (m)
ΔP _{b(x)}	Trans-membrane pressure at each point along the membrane length, (atm)
Δπ _{s(x)}	The osmotic pressure difference at each point along the membrane length, (atm)

commonly used cross flow velocity is laminar, but the separating material (fibre mesh) can serve as a promoter of turbulence, and thus decreases concentration polarisation in the membrane by reducing the membrane boundary layer without an excessive decrease in pressure (Karabelas et al., 2018). The mesh also serves as a buffer for the isolation of the membrane layers. The method of fluid separation begins with the fluid pumping under pressure to push the fluid into the pores, thus depositing on the permeate side at the end of the tube. A schematic diagram of a spiral wound module of RO process is presented in Fig. 1.

The semi-permeable membranes including the spiral wound module of RO process have been used to treat wastewater of a number of industries including textile, dairy, tannery, and pharmaceutical industries to remove several pollutants such as copper, nitrate, sulphate and acrylonitrile (Obotey Ezugbe, and Rathilal, 2020). Phenol, which is highly toxic, can be found in the wastewater of several industrial practices (Magdy et al., 2021). Several researchers tested the feasibility of spiral wound RO process for the removal of phenol from wastewater (Srinivasan et al., 2010; Sundaramoorthy et al., 2011; Al-Obaidi et al., 2017a; Al-Huwaidi et al., 2021). For instance, Al-Obaidi et al. (2017a) evaluated the removal of phenol from synthesised wastewater from varying the operating conditions of the spiral wound RO process. The investigated operating parameters include the inlet phenol concentration, feed pressure and feed flowrate. This simulation confirmed the

necessity of utilising an optimum feed concentration of phenol to obtain the highest phenol rejection. However, to the best knowledge of the authors, the investigation of membrane design parameters of spiral wound module including membrane length, width and feed spacer channel and consequent optimal operating conditions of temperature, pressure and concentration have yet to be concurrently appraised. This study attempts to resolve this gap by developing a simulation model for the removal of phenol from wastewater using a spiral wound RO module. Particular attention will be paid to the careful selection of optimal operating conditions which will yield an improved removal of pollutant (phenol) from wastewater.

2. RO process modelling

This section presents assumptions and the methodology process for modelling elements of the RO process. This model selected is that developed by Al-Obaidi et al. (2017b) as described below.

2.1. Assumptions

The following assumptions were made to aid in the development of the process model:

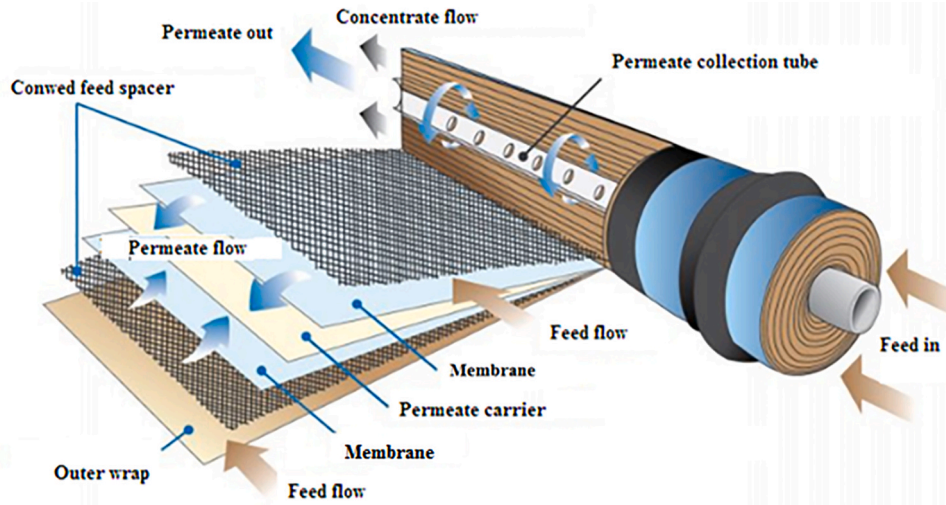


Fig. 1. A schematic diagram of a spiral wound module of RO process (Al-Obaidi, 2019) .

- The Spiegler-Kedem model's validity.
- Darcy's law is valid when the friction parameter is used to describe the pressure drop.
- At the permeate side, a constant pressure of 1 atm is assumed.
- There is minimal curvature of the flat membrane sheet.
- The channel of permeate assumes a constant concentration of solute, and the average value is calculated amounting to that of the solution concentration inlets and outlets.
- For one-dimensional transport, the model is studied
- For the computation, the fundamental assumption is that the process is isothermal.

2.2. Model equations

Al-Obaidi et al. (2017b) developed a one-dimensional model based on the definition of the molar solvent and volumetric solvent fluxes $J_{W(x)}$ and $J_{s(x)}$. The following equations depict the x-axis fluxes across any point of the membrane (all details for each variable can be found in the Nomenclature).

$$J_{W(x)} = L_p (\Delta P_{b(x)} - (\sigma \Delta \pi_{s(x)})) \quad (1)$$

$$J_{s(x)} = J_W (1 - \sigma) C_s^{\sim} + \omega \Delta \pi_{s(x)} \quad (2)$$

The average solute concentration on the feed side of membrane is calculated using the following equation.

$$C_{s(av)}^{\sim} = \frac{C_{s(0)}^{\sim} + C_{s(L)}^{\sim}}{2} \quad (3)$$

$$C_{s(0)}^{\sim} = \frac{C_{s(0)} - C_{p(av)}}{\ln\left(\frac{C_{s(0)}}{C_{p(av)}}\right)}, C_{s(L)}^{\sim} = \frac{C_{s(L)} - C_{p(av)}}{\ln\left(\frac{C_{s(L)}}{C_{p(av)}}\right)} \quad (4)$$

The osmotic pressure difference can be found using the following equation at any point through the membrane.

$$\Delta \pi_{s(x)} = RT_b (C_{W(x)} - C_{p(av)}) \quad (5)$$

Eq. (5) is substituted into Eq. (2) to facilitate the calculation of the solute molar flux across any point of the membrane.

$$J_{s(x)} = J_{W(x)}(1 - \sigma)C_{s(av)}^{\sim} + \omega RT_b (C_{W(x)} - C_{p(av)}) \quad (6)$$

Eq. (6) incorporates two terms: convection, which is produced by the connection between the solute and solvent, and is shown by the first term; and diffusive solute flow, which is shown by the second term in the equation.

Because the solute flow is smaller than the volumetric solvent flux, it

can be summarised into the following equation.

$$J_{s(x)} = J_{W(x)} C_{p(av)} \quad (7)$$

Using the permeate, feed pressure the trans-membrane pressure difference at any point of the membrane can be calculated using Eq. (8).

$$\Delta P_{b(x)} = (P_{b(x)} - P_p) \quad (8)$$

Eq. (9) is constructed by substituting Eq. (7) into Eq. (2), then rearranging it to find the osmotic pressure difference at any point across the membrane.

$$\Delta \pi_{s(x)} = \left(\frac{J_{W(x)} C_{p(av)}}{\omega} \right) - \left(\frac{J_{W(x)} (1 - \sigma) C_{s(av)}^{\sim}}{\omega} \right) \quad (9)$$

Eq. (9) can be substituted into Eq. (1) in order to find the water flux through the membrane at any point.

$$J_{W(x)} = L_p \left[\Delta P_{b(x)} - \sigma \left(\left(\frac{J_{W(x)} C_{p(av)}}{\omega} \right) - \left(\frac{J_{W(x)} (1 - \sigma) C_{s(av)}^{\sim}}{\omega} \right) \right) \right] \quad (10)$$

Eq. (10) is further simplified to give:

$$J_{W(x)} = \frac{L_p (\Delta P_{b(x)})}{1 + \left(\frac{\sigma C_{p(av)} L_p}{\omega} \right) - \left(\frac{C_{s(av)}^{\sim} (1 - \sigma) L_p \sigma}{\omega} \right)} \quad (11)$$

The flowrate of brine would naturally drop as it travels through the membrane, and this can be predicted as:

$$\frac{d^2 F_{b(x)}}{dx^2} = -W J_{W(x)} \quad (12)$$

The second derivative may be deduced by combining Eq. (10) and Eq. (12), as follows

$$\frac{d^2 F_{b(x)}}{dx^2} = \frac{-W L_p \frac{dP_{b(x)}}{dx}}{1 + \left(\frac{\sigma C_{p(av)} L_p}{\omega} \right) - \left(\frac{C_{s(av)}^{\sim} (1 - \sigma) L_p \sigma}{\omega} \right)} \quad (13)$$

A pressure decrease should be noted due to friction along the wall membrane. The expression of this decrease in the equation is Darcy's law.

$$\frac{dP_{b(x)}}{dx^2} = -b F_{b(x)} \quad (14)$$

Substituting Eq. (14) into Eq. (13), gives:

$$\frac{d^2 F_{b(x)}}{dx^2} = \frac{W L_{pb} F_{b(x)}}{1 + \left(\frac{\sigma C_{p(av)} L_p}{\omega} \right) - \left(\frac{C_{s(av)}^{\sim} (1 - \sigma) L_p \sigma}{\omega} \right)} \quad (15)$$

$$\frac{d^2 F_{b(x)}}{dx^2} = \frac{L_p}{Z} F_{b(x)} \tag{16}$$

The combination of Eqs. (15) and 16 is then rearranged and simplified to find parameter Z

$$Z = \frac{1 + \left(\frac{\sigma C_{p(av)} L_p}{\omega}\right) - \left(\frac{C_{s(av)}^{(1-\sigma)} L_p \sigma}{\omega}\right)}{Wb} \tag{17}$$

$$F_{b(x)} = e^{rx} \text{ where, } r = \pm \sqrt{\frac{L_p}{Z}} \tag{18}$$

The boundary condition from Eq. (16) is used to generate the final solution as follows

$$F_{b(L)} = \frac{F_{b(0)} \left(e^{\sqrt{\frac{L_p}{Z}} L} - e^{-\sqrt{\frac{L_p}{Z}} L} \right) + F_{b(0)} \left(e^{\sqrt{\frac{L_p}{Z}} (L-x)} - e^{-\sqrt{\frac{L_p}{Z}} (L-x)} \right)}{\left(e^{\sqrt{\frac{L_p}{Z}} L} - e^{-\sqrt{\frac{L_p}{Z}} L} \right)} \tag{19}$$

Eq. (19) is substituted into Eq. (14). With the boundaries introduced, it can be integrated into the following equation

$$P_{b(x)} = P_{b(0)} - \left(\frac{b}{\sqrt{\frac{L_p}{Z}} \left(e^{\sqrt{\frac{L_p}{Z}} L} - e^{-\sqrt{\frac{L_p}{Z}} L} \right)} \right) \left\{ \left(F_{b(L)} \left(e^{\sqrt{\frac{L_p}{Z}} x} + e^{-\sqrt{\frac{L_p}{Z}} x} - 2 \right) - F_{b(0)} \left(e^{\sqrt{\frac{L_p}{Z}} (L-x)} + e^{-\sqrt{\frac{L_p}{Z}} (L-x)} \right) - \left(e^{\sqrt{\frac{L_p}{Z}} L} - e^{-\sqrt{\frac{L_p}{Z}} L} \right) \right) \right\} \tag{20}$$

Eq. (21) yields from equating Eq. (12) to the derivative of Eq. (19), as follows

$$J_{W(x)} = \left(\frac{\sqrt{\frac{L_p}{Z}}}{W \left(e^{\sqrt{\frac{L_p}{Z}} L} - e^{-\sqrt{\frac{L_p}{Z}} L} \right)} \right) \left\{ \left[F_{b(0)} \left(e^{\sqrt{\frac{L_p}{Z}} (L-x)} + e^{-\sqrt{\frac{L_p}{Z}} (L-x)} \right) \right] \left[F_{b(L)} \left(e^{\sqrt{\frac{L_p}{Z}} x} + e^{-\sqrt{\frac{L_p}{Z}} x} \right) \right] \right\} \tag{21}$$

Using the boundary limits and equating equations to solve the transmembrane pressure at each point across the membrane.

$$\Delta P_{b(x)} = \frac{\sqrt{\frac{L_p}{Z}} Z b \left\{ \left[F_{b(0)} \left(e^{\sqrt{\frac{L_p}{Z}} (L-x)} + e^{-\sqrt{\frac{L_p}{Z}} (L-x)} \right) \right] - \left[F_{b(L)} \left(e^{\sqrt{\frac{L_p}{Z}} x} + e^{-\sqrt{\frac{L_p}{Z}} x} \right) \right] \right\}}{L_p \left(e^{\sqrt{\frac{L_p}{Z}} L} - e^{-\sqrt{\frac{L_p}{Z}} L} \right)} \tag{22}$$

To determine the brine output flowrate, it is necessary to rearrange Eq. (22), as shown below

$$F_{b(L)} = \left(\frac{F_{b(0)} \left(e^{\sqrt{\frac{L_p}{Z}} L} - e^{-\sqrt{\frac{L_p}{Z}} L} \right)}{2} \right) - \left(\frac{\Delta P_{b(0)} \sqrt{\frac{L_p}{Z}} \left(e^{\sqrt{\frac{L_p}{Z}} L} - e^{-\sqrt{\frac{L_p}{Z}} L} \right)}{2b} \right) \tag{23}$$

Using Eq. (24) will determine the solute concentration along the x-axis of the membrane

$$\frac{d \left(\frac{C_{s(x)} F_{b(x)}}{t_f W} \right)}{dx} = - \left(\frac{J_{W(x)} C_{p(av)}}{t_f} \right) + \left(\frac{J_W C_{s(x)}}{t_f} \right) + \frac{d}{dx} \left(D_{b(x)} \left(\frac{dC_{s(x)}}{dx} \right) \right) \tag{24}$$

The accumulation of the impermeable solute on the membrane surface may also be addressed using the concept of concentration polarisation

$$\frac{(C_{W(x)} - C_{p(av)})}{(C_{s(c)} - C_{p(av)})} = \exp \left(\frac{J_{W(x)}}{k(x)} \right) \tag{25}$$

The combination of Eqs. (25) and (7) is first required to work out the concentration polarisation

$$J_{W(x)} C_{p(av)} = C_{s(av)}^{(1-\sigma)} (1-\sigma) J_{W(x)} + \omega RT_b (C_{s(x)} - C_{p(av)}) e^{\left(\frac{J_{W(x)}}{k(x)} \right)} \tag{26}$$

To get the average permeate solute, Eq. (26) is rearranged as shown below

$$C_{p(av)} = \left(\frac{C_{s(av)}^{(1-\sigma)} (1-\sigma) J_{W(x)} + \omega RT_b C_{s(x)} e^{\left(\frac{J_{W(x)}}{k(x)} \right)}}{J_{W(x)} + \omega RT_b e^{\left(\frac{J_{W(x)}}{k(x)} \right)}} \right) \tag{27}$$

To reduce Eq. (27) into Eq. (28), it is assumed that the reflection

coefficient is equal to 1

$$C_{p(av)} = \left(\frac{\omega RT_b C_{s(x)} e^{\left(\frac{J_{W(x)}}{k(x)}\right)}}{J_{W(x)} + \omega RT_b e^{\left(\frac{J_{W(x)}}{k(x)}\right)}} \right) \quad (28)$$

It is possible to calculate the average permeate solute concentration using the Solution-diffusion model by expressing Eq. (28) as Eq. (29)

$$C_{p(av)} = \left(\frac{B_s C_{s(x)} e^{\left(\frac{J_{W(x)}}{k(x)}\right)}}{J_{W(x)} + B_s e^{\left(\frac{J_{W(x)}}{k(x)}\right)}} \right) \quad (29)$$

The separation effectiveness of the membrane is derived from the solute rejection coefficient, which is a measure of separation as follows

$$Rej_{(av)} = \left(\frac{C_{s(L)} - C_{p(av)}}{C_{s(L)}} \right) x \quad (30)$$

Additionally, to get the overall flow rate, the sum of all permeated water along the x-axis can be calculated as follows

$$\frac{dF_{p(x)}}{dx} = WJ_{W(x)} \quad (31)$$

$$F_{o(total)} = F_{p(L)} \quad (32)$$

It is worth noting that the coefficient of mass transmission is essentially based on the solvent flux, flow rate, solute concentration and solvent, and solution properties. In addition, the coefficient of mass transfer varies along the x-axis dimension. The following equation helps quantify the impact of each variable.

$$k_{(x)} = c_1 [Re_{p(x)} Re_{f(x)} C_{m(x)} Sc_{p(x)} Sc_{f(x)}]^2 \quad (33)$$

$$Sh = \frac{2t_f k_{(x)}}{D_{b(x)}} \quad (34)$$

$$Re_{p(x)} = \frac{2t_p \rho_{p(x)} J_{W(x)}}{\mu_{p(x)}} \quad \text{and} \quad Re_{f(x)} = \frac{2\rho_{f(x)} F_{b(x)}}{W\mu_{f(x)}} \quad (35)$$

$$C_{m(x)} = \frac{C_{s(x)}}{\rho_m} \quad (36)$$

$$Sc_{p(x)} = \frac{\mu_{p(x)}}{\rho_{p(x)} D_{p(x)}} \quad \text{and} \quad Sc_{f(x)} = \frac{\mu_{f(x)}}{\rho_{f(x)} D_{f(x)}} \quad (37)$$

The permeate concentration along the x-axis and the molar density of water have a corresponding coefficient of solute diffusion. The equation used to derive the mass transfer coefficients is given below

$$k_{(x)} = 1.177 \left(\frac{F_{b(x)} D_{b(b)}^2}{t_f^2 WL} \right)^{0.333} \quad (38)$$

Deducing the values of constants is possible by showing specific variables. The phenol total mass transfer coefficient is determined as follows

$$k_{(x)} = \frac{6.5045 D_{f(x)}^{0.9995}}{t_f} \left(\frac{F_{b(x)} t_p J_{W(x)} C_{s(x)}}{W \rho_m D_{p(x)}} \right)^{0.0005} \quad (39)$$

Table 1
Characteristics of the selected membrane.

Membrane characteristics	
Make	Ion Exchange, India
Membrane Material	Thin-film composite (TFC) Polyamide
Module configuration	Spiral wound

Table 2

Membrane design specifications of selected modules for variable membrane length.

Membrane design specifications	Module		
	Base Case	1	2
Module length (m)	0.45	0.4	0.5
Module width (m)	1.667	1.667	1.667
Feed spacer thickness (m)	8.50E-04	8.50E-04	8.50E-04
Permeate spacer thickness (m)	7.80E-04	7.80E-04	7.80E-04

3. Membrane characteristics and operating conditions

Membrane properties have a significant impact on the process ability to operate at optimal conditions. The use of the correct membrane is thus very important. This section discusses the evaluation of the influence of different design parameters of the membrane including length, width, feed spacer thickness, and permeate spacer thickness on the phenol removal from wastewater. It seeks to identify optimal values via the simulation-based model developed. Table 1 shows the membrane characteristics of an Ion Exchange membrane. The simulation will be carried out considering a set of inlet conditions of 10 atm of pressure, 8.5E-03 kmol/m³ of phenol feed concentration, 3.33E-4 m³/s of feed flowrate, and 32.2 °C of temperature.

The current simulation includes the variation of one design parameter of the membrane while other design parameters are fixed at the original base case values. The original membrane specifications are denoted as the base case module, while Modules 1 and 2 denote two different membrane specifications tested with specified length, width, and feed spacer thickness. In this regard, the module length has been taken as 0.45 m, 0.4 m, and 0.5 m for the base case, module 1 and module 2, respectively. The module width has been taken as 1.667 m, 1.0 m, and 2.0 m for the base case, module 1 and module 2, respectively. Also, the feed spacer thickness has been taken as 8.50E-04, 8.0E-04, and 9.0E-04 for or the base case, module 1 and module 2, respectively.

4. Results and discussion

4.1. Analysis of membrane design parameters

To critically investigate the influence of membrane length on the performance indicators of the spiral wound RO process for the phenol removal from wastewater, Modules 1 and 2 are proposed. They correspond to a lower and higher membrane length compared to the base case respectively as shown in Table 2. The membrane width, feed spacer thickness and permeate spacer thickness of the original base case are maintained in Modules 1 and 2. Additionally, the length of each membrane in each module is split into 5 subsections based on the membrane length selected. For instance, each subsection is 0.1 m for 0.5 m membrane length. This is in line with using a one-dimensional simulation model (Section 3).

Fig. 2 illustrates the pressure and phenol feed concentration fluctuation on the membrane length for three different modules, while the RO process is operating in a steady state condition. The pressure drop, due to friction, results in a decreased feed pressure along the membrane length. Clearly, the pressure gradient between the feed and permeate channels is at its greatest at the entry of the membrane and at its lowest at the end of the unit. Due to water being absorbed by the membrane, the phenol concentration gradually increases in the sub-sections of the feed channel across the membrane.

Fig. 2 clearly shows that employing the two proposed Modules 1 and 2 of the membrane length and corresponding dimensions (Table 2) has no significant impact on the distributions of feed pressure and phenol concentration across the membrane, where similar behaviours can be noticed. However, Module 1 has the best feed pressure across the membrane length, and this yields a higher net driving pressure to

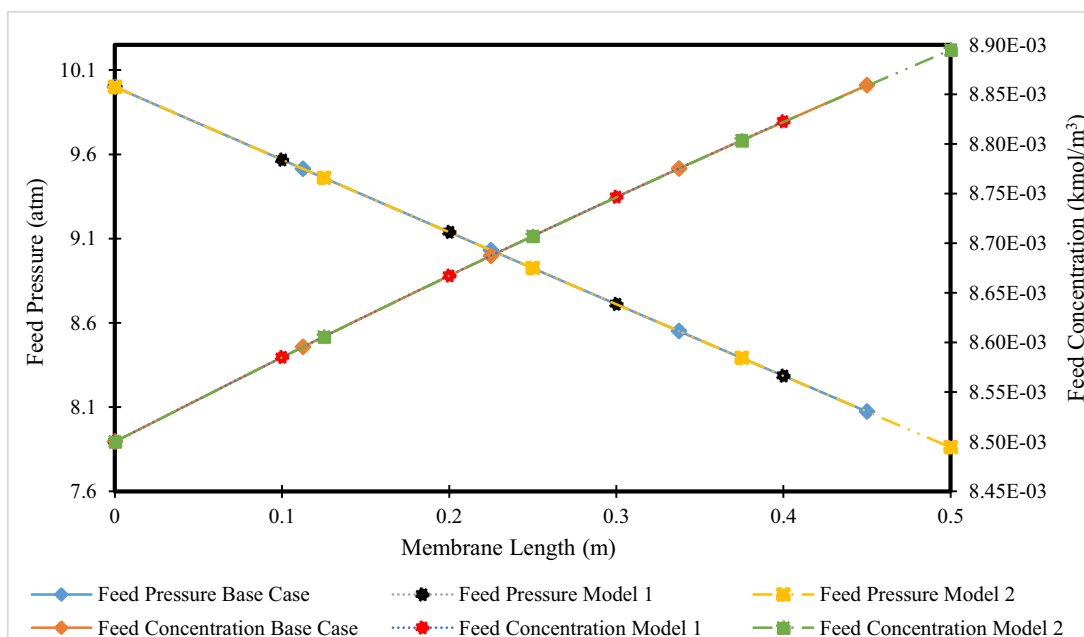


Fig. 2. Feed pressure and phenol concentration along the membrane length with varying membrane length.

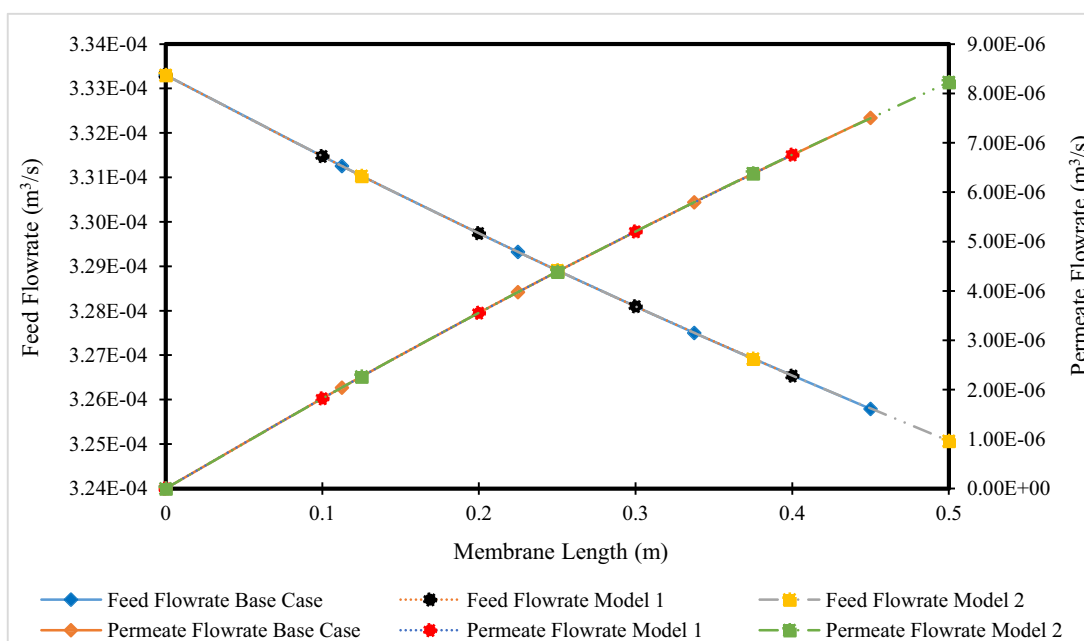


Fig. 3. Feed and permeate flowrates along the membrane length with varying membrane length.

generate a higher water flux through the membrane pores compared to the base case and Module 2. This is due to the lower membrane length of Module 1. As the membrane length increases, it can be observed that the feed pressure of Module 1 is comparable to the feed pressure of base case and Module 2. This is another indication of the clear influence of lowering the membrane length to gain a higher feed pressure along the membrane length compared to a larger membrane length. On the other hand, Module 2 with the largest values of membrane length appears to have the highest phenol concentration throughout the membrane length compared to the base case and Module 1. Module 2 has the lowest feed pressure and lowest pressure driving force. This implies a lower water flux with a higher accumulation of phenol on the membrane wall that explains the increase of feed concentration throughout the membrane

length. The variation of phenol concentration between the three modules is clearly visible at the end of the membrane length.

The above results confirm that Module 1 yields higher phenol removal from wastewater due to its high feed pressure driving force compared to the other modules tested.

It is crucial to look at the behaviour of the feed flow rate across the membrane length in order to realize the behaviour of the phenol concentration depicted in Fig. 2. Fig. 3 shows the distribution of the feed flowrate in the feed channel and permeate flowrate in the permeate channel throughout the subsections of the feed channel for the modules of different membrane length tested. The feed flowrate decreases throughout the membrane channel because of water infiltration throughout the membrane, causing feed velocity to be lowered and feed

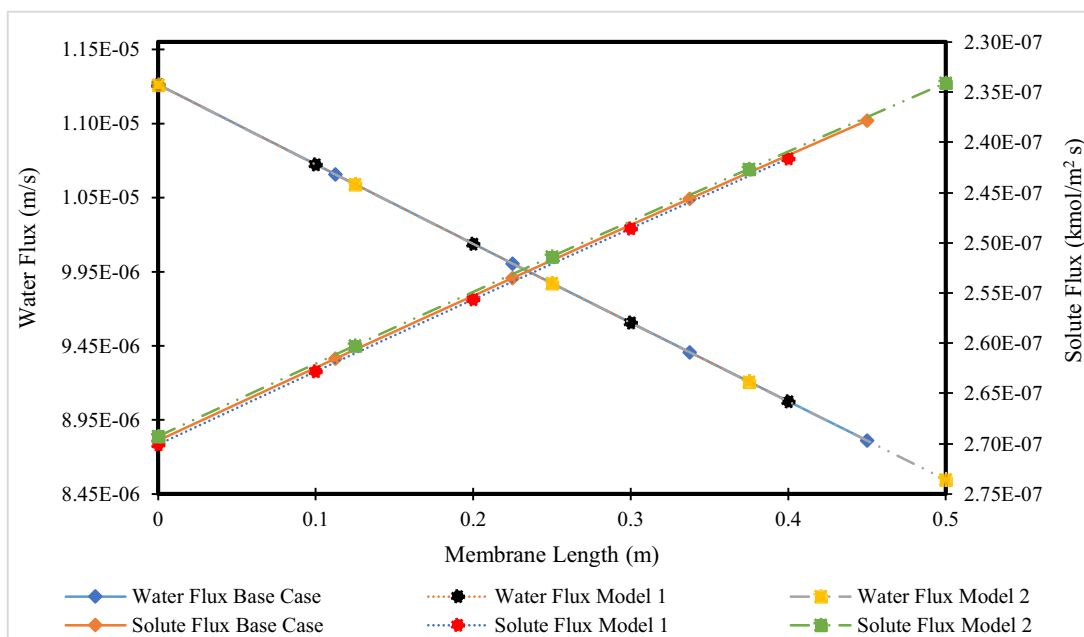


Fig. 4. Water and solute fluxes along the membrane length with varying membrane length.

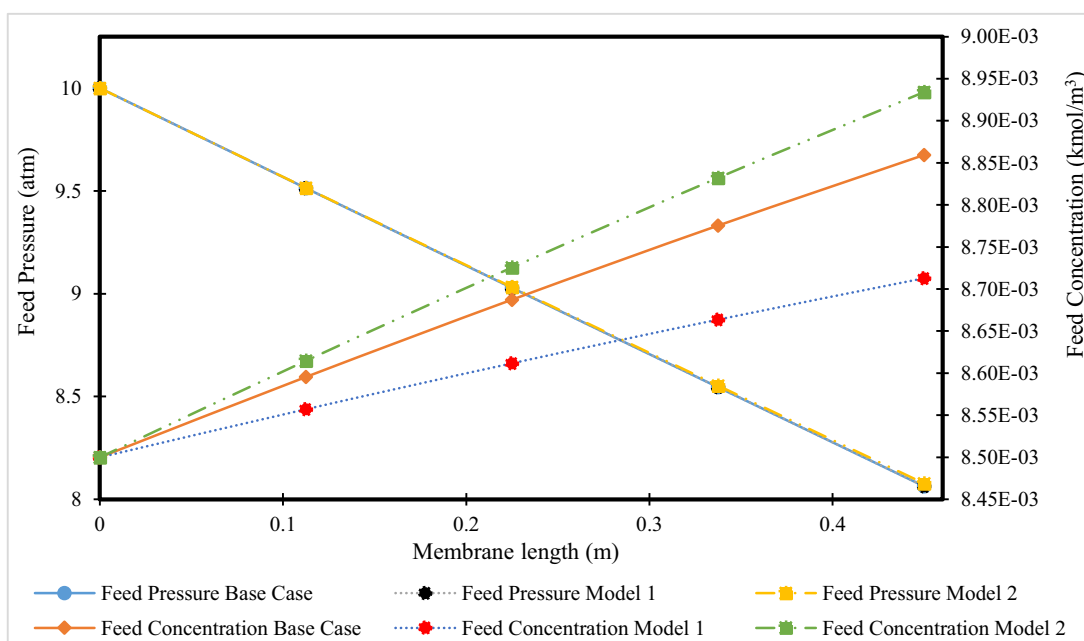


Fig. 5. Feed pressure and phenol concentration along the membrane length with varying membrane width.

Table 3

Membrane design specifications of selected modules for variable membrane width.

Membrane design specifications	Module		
	Base Case	1	2
Module length (m)	0.45	0.45	0.45
Module width (m)	1.667	1.0	2.0
Feed spacer thickness (m)	8.50E-04	8.50E-04	8.50E-04
Permeate spacer thickness (m)	7.80E-04	7.80E-04	7.80E-04

concentration to be raised as seen in Fig. 2. More importantly, the membrane length has a clear influence on the feed and permeate flowrates. Specifically, the application of the two proposed modules and the

base case of different membrane length, has a clear effect on the distribution of feed and permeate flowrates. In this regard, Module 1 is characterised by the highest feed flowrate compared to the base case and Module 2. This is due to it having the lowest values of membrane length which upgrade the feed flowrate. Having the highest feed flowrate implies the highest rate of disturbance that incorporates the lowest phenol concentration compared to the other modules tested. Accordingly, Module 1 provides the best option due to its higher feed flowrate along the membrane length, which accelerates the water flux and increases phenol rejection.

As the pressure drops along the membrane length due to friction, the net pressure driving force is reduced, and this causes a decrease in the water and solute fluxes through the membrane. Fig. 4 shows this for the

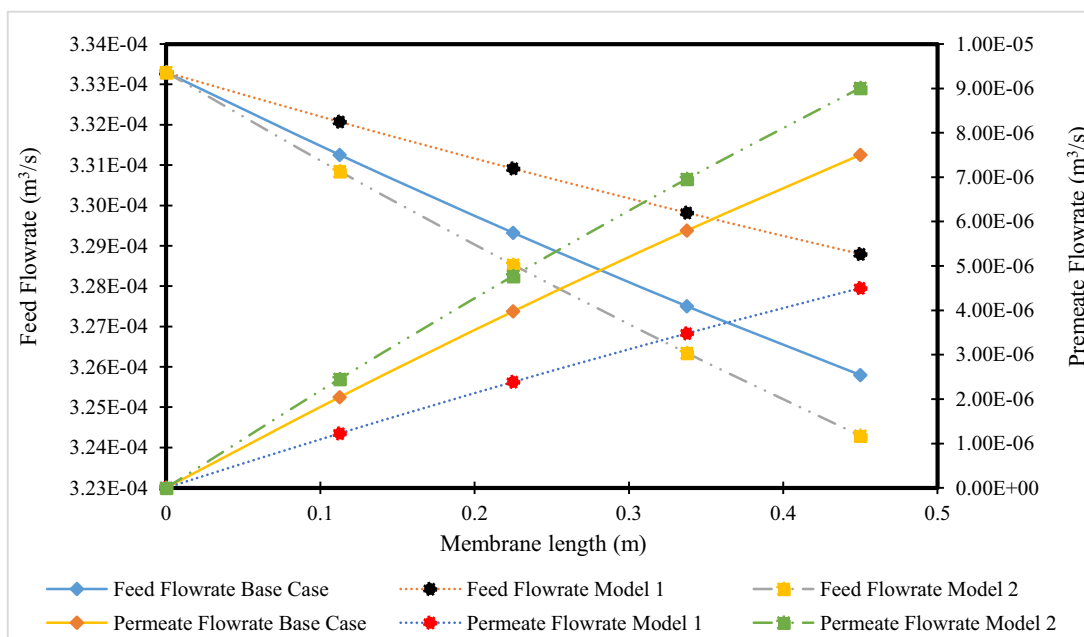


Fig. 6. Feed and permeate flowrate along the membrane length with varying membrane width.

three modules studied. In particular, Fig. 4 also shows the results of Fig. 2 where the maximum water flux using Module 1 was achieved at the lowest value of membrane length. The base case has the second order of water flux while Module 2 has the lowest water flux with the biggest membrane length. Furthermore, the solute flux results are commensurate with the water flux results. These exhibit a clear increase of the water flux as the membrane length decreases due to an increase of accumulated phenol on the membrane surface. Again, changing the membrane length has little influence on water and solute fluxes through the membrane pores along the membrane length. It can therefore be said that Module 1 yields higher phenol removal from wastewater than the base case or Module 2, as clearly shown in Figs. 2, 3, and 4.

To analyse the effect of membrane width (at fixed membrane length, feed spacer thickness, permeate spacer thickness) on the related

performance indicators of RO process in respect of the removal of phenol from wastewater, Fig. 5 depicts the distribution in feed pressure and phenol concentration throughout the membrane length for three different modules of different membrane width including the base case module (Table 3).

Clearly, it can be seen that changing the membrane width has little influence on the feed pressure distribution but considerable influence on the feed concentration distribution.

Fig. 5 shows that having the highest membrane width (Module 2) would yield the highest phenol concentration along the membrane subsections compared to the base case and Module 1. This can be attributed to a clear reduction of the feed flowrate in the feed channel as the width of membrane increases. Thus a reduction of disturbance rate is mostly expected due to lowering the feed flow rate that causes an

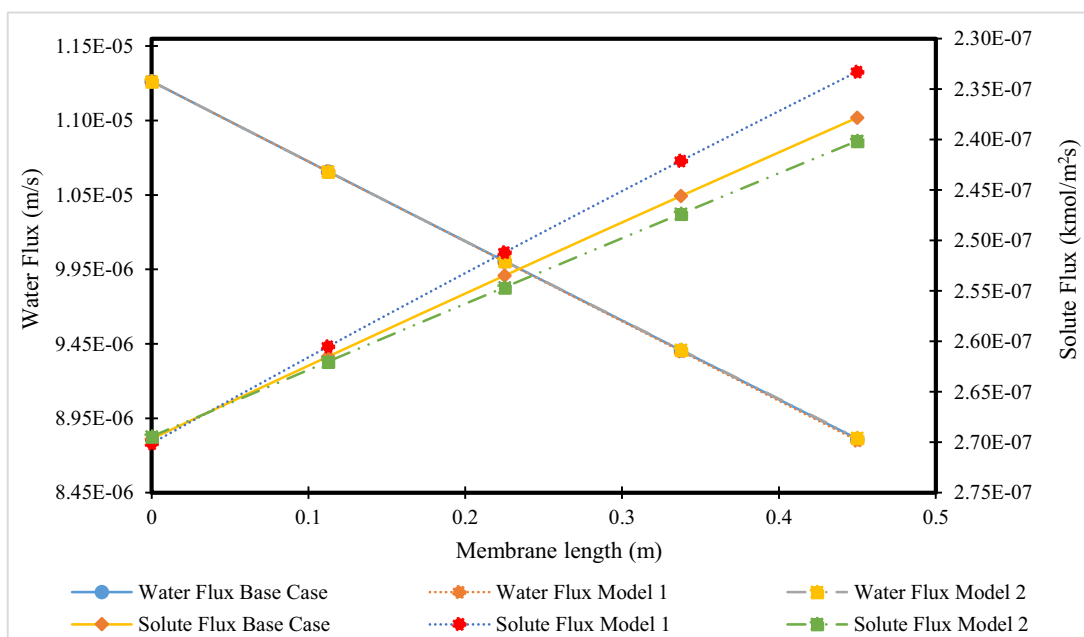


Fig. 7. Water and solute flux along the membrane length with varying membrane width.

Table 4
Membrane design specifications of selected modules for variable membrane feed spacer thickness.

Membrane design specifications	Module		
	Base Case	1	2
Module length (m)	0.45	0.45	0.45
Module width (m)	1.667	1.667	1.667
Feed spacer thickness (m)	8.50E-04	8.00E-04	9.00E-04
Permeate spacer thickness (m)	7.80E-04	7.80E-04	7.80E-04

increase of phenol concentration in each subsection along the membrane length of Module 2. Statistically, phenol concentration at the membrane end is raised from 8.86E-03 (Base Case) to 8.93E-03 kmol/m³ (Model 2) when the membrane width is increased from 1.667 m to 2.0 m. More importantly, the increased feed concentration results in an increase in osmotic pressure, and in a decrease in water flux and solute rejection. It is therefore important to deploy Module 1 of the lowest membrane width in order to guarantee the reduction of the accumulated phenol on the membrane surface, which in turn would lead to fouling and scaling problems.

It can be affirmed that using Module 1 at the lowest value of membrane width would delay the solute flux and therefore would limit the permeate concentration of phenol in the permeate channel. Thus, Module 1 yields highest phenol rejection.

Fig. 6 shows that increasing the width of the membrane lowers the feed flowrate more quickly and raises the permeate flowrate equally. The feed flowrate is 3.26E-4 m³/s in the basic scenario; when the membrane width is increased, and the feed flowrate decreases to 3.24E-04 m³/s. In the same trend, the permeate flowrate is 7.51E-06 in the basic scenario, but it rises to 9.01E-06 when the width is increased to 2.0 m in Module 2. Based on these results, it can be confirmed that using a high membrane width would generate the lowest feed flowrate along the membrane length and vice versa. This is due to availability of a higher space for the particle moving throughout the membrane with increasing the membrane width, thus decreasing the feed flow rate. Thus, it is recommended to select Module 1 since it incorporates the highest feed flowrate along the membrane length that would cause a higher rate of mixing and turbulence. This implies a higher rate of water flux and lower permeate phenol concentration.

Water and solute fluxes decrease throughout the membrane length

when the pressure drops due to friction, which in turn reduces the net pressure driving force. Varying the membrane width had no effect on water flux but did have an effect on solute flux as shown in Fig. 7. At the membrane end, the solute flux was 2.38E-07 kmol/m² s in the base case, 2.40E-07 kmol/m² s in Module 2 with the increased width, and 2.33E-07 kmol/m² s in Module 1 with the reduced width. The dominant low solute flux of Module 1 can be attributed to the high rate of disturbance with the highest values of feed flow rate. This in turn would retard the possibility of passing phenol molecules through the membrane wall to be transferred to the permeate channel. This confirms the effectiveness of Module 1 as it identifies the best design for the highest removal of phenol from wastewater.

According to the above results, Module 1 yields maximum phenol rejection due to having the highest feed flow rate of the lowest solute flux.

The feed spacer thickness is the next variable to be tested using three modules of different values of feed spacer thickness for the removal of phenol from wastewater. Table 4 shows the dimensions of the feed spacer for the base case and the Modules 1 and 2 considered. In this regard, Module 1 has the lowest feed spacer thickness while Module 2 has the larger feed spacer thickness. However, the other dimensions of membrane length, membrane width, permeate spacer thickness are selected the same as the base case.

Increasing the feed spacer thickness has resulted in a minor change in water flux through the membrane length (Fig. 8). However, Fig. 8 shows a considerable variation between the solute flux of the three modules tested. In this regard, the lowest feed spacer thickness of Module 1 has the lowest rate of solute flux with a relatively a considerable difference against the base case module and Module 2. This is due to the possibility of gaining a higher feed flowrate along the membrane length due to reducing the overall area of feed flowing.

Again, the simulation of different modules of variable feed spacer

Table 5
Temperature specification of three selected models.

Parameter	Module		
	Base case	1	2
Temperature (°C)	32.2	25	40

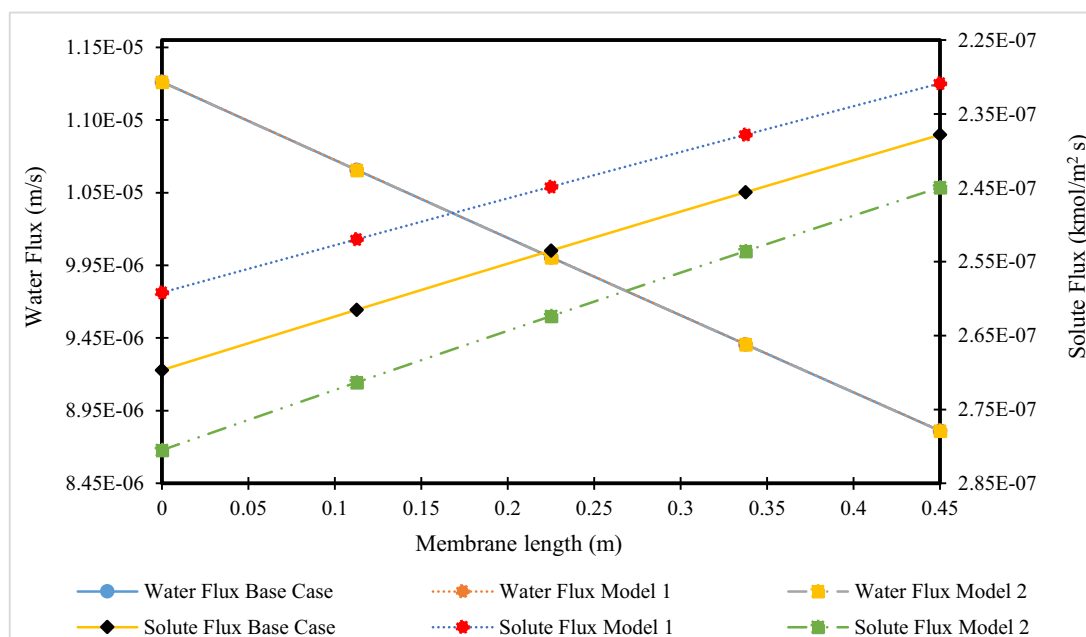


Fig. 8. Water and solute flux along the membrane length with varying feed spacer thickness.

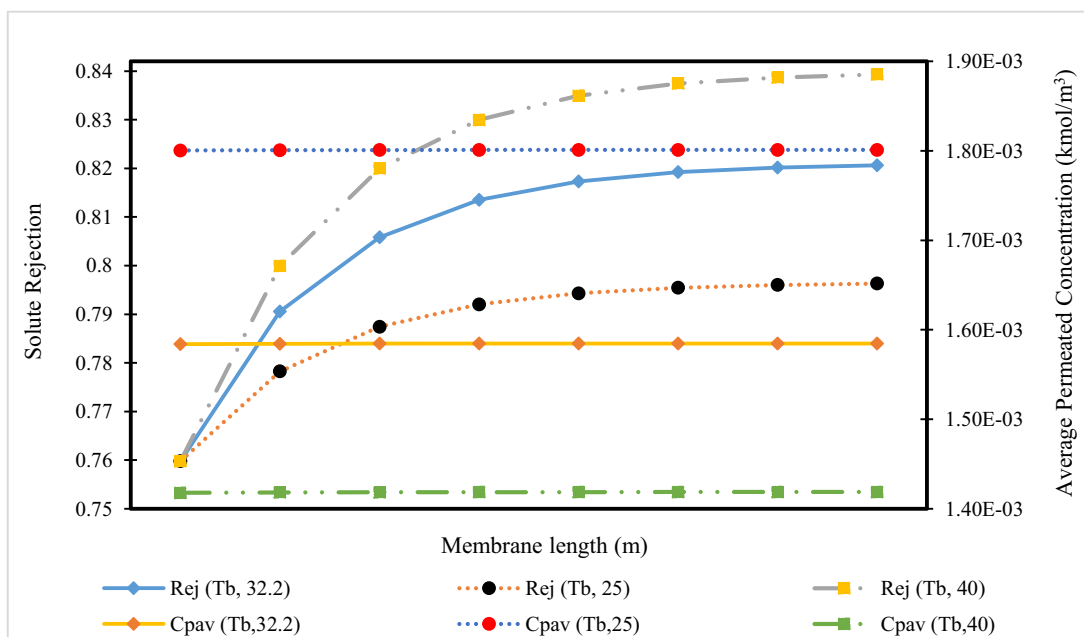


Fig. 9. Temperature effect on phenol rejection and average permeate concentration of three different models.

Table 6

Pressure specification of three selected models.

Parameter	Module		
	Base Case	1	2
Inlet pressure (atm)	10	8	12

thickness readily confirm the viability of Module 1 with the lowest feed spacer thickness due to having the lowest solute flux and therefore the maximum phenol rejection.

4.2. Temperature simulation

Having realised an appropriate membrane design for Module 1 that

yields improved performance, this section explores the impact of varying the operating temperature in three models; namely the base case and Modules 1 and 2. It is expected that the variation of temperature would affect both water and solute fluxes through the membrane pores as well as the overall phenol removal from wastewater. Increasing the temperature would reduce the density and viscosity of the fluid besides increasing the water diffusivity which increases the mobility of the

Table 7

Concentration specification.

Parameter	Base Case	Model 1	2
	Inlet concentration (kmol/m ³)	8.5E-03	7.0E-03

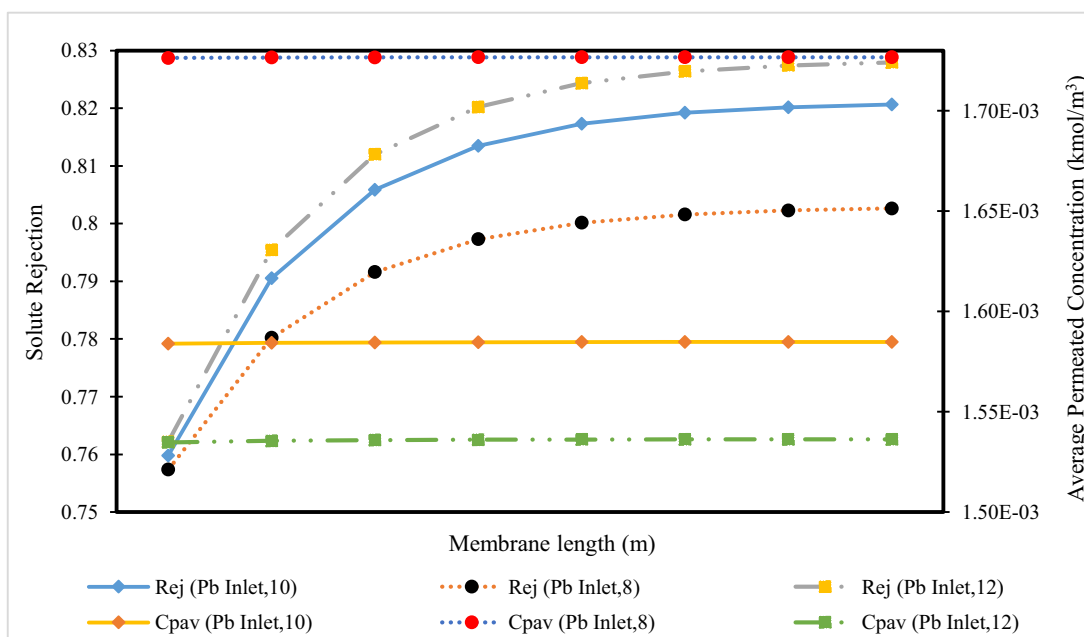


Fig. 10. Pressure effect on phenol rejection and average permeate concentration of three different models.

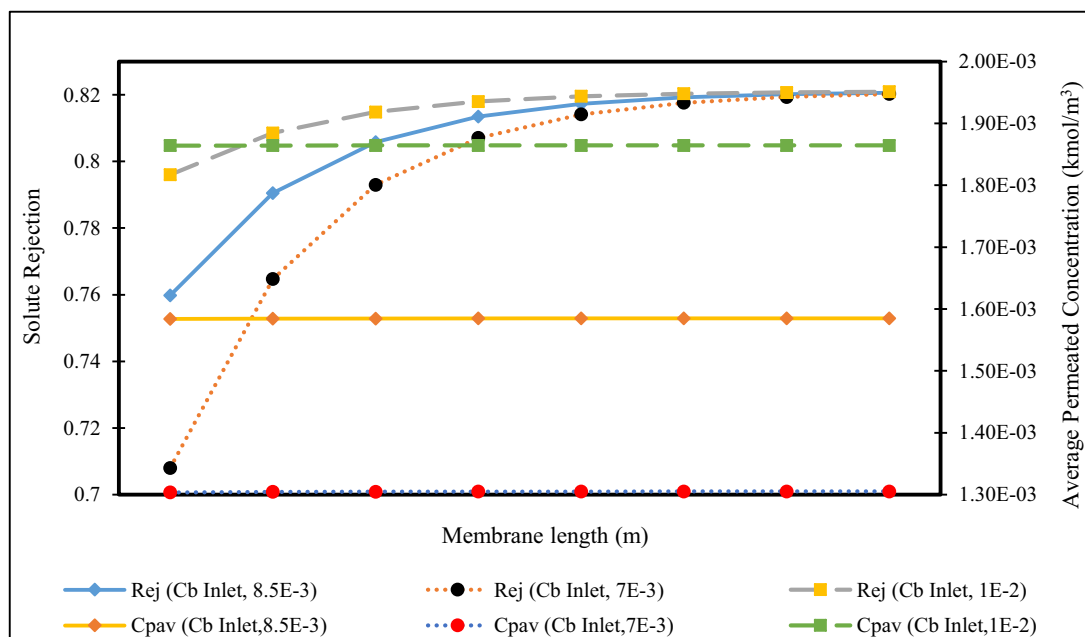


Fig. 11. Concentration effect on solute rejection and average permeate concentration.

particles and therefore increases water and solute fluxes through the membrane pores (Goosen et al., 2002). The specifications of the selected models are given in Table 5. The other operating parameters of feed phenol concentration, pressure flowrate will be fixed at $8.5E-3$ kmol/m^3 , of 10 atm, and $3.33E-4$ m^3/s , respectively.

As shown in Fig. 9, raising the temperature increases solute rejection and decreases the average permeate concentration across the membrane. Changing the temperature has a substantial effect on both. When the temperature rises, the solute flux across the membrane reduces, thus decreasing the average permeate concentration and increasing the quantity of phenol rejected. As stated above, an increase of operating temperature results in a decrease of solution density and viscosity, which explains the increase of water molecules to pass the membrane pores.

4.3. Pressure simulation

This section discusses the variation of operating pressure and its influence on the phenol rejection in the three models tested. This is presented in Table 6 with a fixed set of operating phenol concentration, flowrate, and temperature of $8.5E-3$ kmol/m^3 , $3.33E-4$ m^3/s , and 25 °C, respectively.

Fig. 10 confirms that raising the operating pressure increases solute rejection while reducing the average permeate concentration through the membrane. This is due to increasing the driving force of water flux that reduces the phenol concentration in the permeate channel.

4.4. Concentration simulation

Alternating concentrations of phenol is expected to happen throughout the treatment. Thus, this section focuses on analysing the influence of variable feed concentration at fixed feed pressure, flowrate and temperature 10 atm, $3.33E-4$ m^3/s , and 25 °C, respectively. Table 7 shows the concentration specification of the three selected models.

Fig. 11 shows that increased concentration leads to comparable solute rejection, but to a decreasing average permeate concentration across the membrane. The initial rejection of solutes differed at the start of the membrane owing to the varying concentrations of each model. However, they all end up with the same value at the membrane end. The increase of phenol concentrations in the feed channel significantly

increases the overall osmotic pressure. This in turn retards the water flux and decreases the phenol rejection due to increasing the phenol concentration in the permeate channel Al-Obaidi et al., 2020b.

The only problem remaining is that the possible fouling is not taken into consideration. It is thought that by expanding the model equations to include this term in a dynamic model version, more reliable values of phenol removal from wastewater especially for different periods of operation can be achieved. Further investigations of different RO process configurations aimed at reducing the permeate production cost per volume will be addressed in further research.

5. Conclusions

Reverse Osmosis is a successful treatment method for the removal of organic pollutants in water reclamation applications. In this paper, a one-dimensional steady state model based on the irreversible thermodynamic principle used for the treatment of wastewater using the spiral-wound RO process. The simulation revealed that the combined membrane width, operating pressure, and feed temperature have a significant effect on phenol removal from wastewater. These variables have most influence on the four distinct parameters that determine an RO membrane performance including the permeate concentration, solute flux, solute rejection and water flux. Specifically, utilising the lowest value of membrane width would delay the solute flux and therefore yields the highest phenol rejection. Increasing the feed pressure would increase the water flux and enhances the phenol rejection. Also, increasing water temperature would enhance water flux and phenol removal due to reducing water density and viscosity. Based on the simulation results and the selected ranges of parameters, the optimal membrane characteristics and operating condition to obtain the maximum removal of phenol from wastewater using a single spiral-wound module of RO process are as follows; 0.4 m, 1.667 m, and $8.0E-04$ m of module length, module width, and feed spacer channel, respectively, and 40 °C, 12 atm, $7.0E-03$ kmol/m^3 of temperature, pressure and phenol concentration, respectively. It can therefore be said that the use of appropriate membrane operating and design parameters yield optimal RO system performance.

Declaration of Competing Interest

None

References

- Al-Huwaidi, J.S., Al-Obaidi, M.A., Jarullah, A.T., Kara-Zaitri, C., Mujtaba, I.M., 2021. Modeling and simulation of a hybrid system of trickle bed reactor and multistage reverse osmosis process for the removal of phenol from wastewater. *Comput. Chem. Eng.* 153, 107452.
- Al-Obaidi, M.A., Kara-Zaitri, C., Mujtaba, I.M., 2017a. Removal of phenol from wastewater using spiral-wound reverse osmosis process: model development based on experiment and simulation. *J. Water Process Eng.* 18, 20–28.
- Al-Obaidi, M.A., Kara-Zaitri, C., Mujtaba, I., 2017b. Modeling of a spiral-wound reverse osmosis process and parameter estimation. *Desalination Water Treat* 69 (1), 93–101.
- Al-Obaidi, M.A., Jarullah, A.T., Kara-Zaitri, C., Mujtaba, I.M., 2018. Simulation of hybrid trickle bed reactor–reverse osmosis process for the removal of phenol from wastewater. *Comput. Chem. Eng.* 113, 264–273.
- Al-Obaidi, M.A., 2019. Modelling, Simulation, and Optimisation of Reverse Osmosis Process with Application in Wastewater Treatment and Food Processing, PhD Thesis. University of Bradford, UK.
- Al-Obaidi, M., Kara-Zaitri, C., Mujtaba, I., 2020a. *Wastewater Treatment by Reverse Osmosis Process. State of the Art and Process Modelling*. CRC Press, Boca Raton. <https://doi.org/10.1201/9781003019343> eBook ISBN 9781003019343.
- Al-Obaidi, M.A., Mustafa, S.N., Malek, K.H., 2020b. Evaluation of phenol removal via a spiral wound reverse osmosis process with different feed concentrations: simulation study. *Water Sci. Technol.* 82 (9), 1885–1895.
- Attarde, D., Jain, M., Singh, P.K., Gupta, S.K., 2017. Energy-efficient seawater desalination and wastewater treatment using osmotically driven membrane processes. *Desalination* 413, 86–100.
- Chaturvedi, N.K., 2022. Comparison of available treatment techniques for hazardous aniline-based organic contaminants. *Appl. Water Sci.* 12 (7), 1–15.
- Goosen, M.F., Sablani, S.S., Al-Maskari, S.S., Al-Belushi, R.H., Wilf, M., 2002. Effect of feed temperature on permeate flux and mass transfer coefficient in spiral-wound reverse osmosis systems. *Desalination* 144 (1–3), 367–372.
- Karabelas, A.J., Koutsou, C.P., Sioutopoulos, D.C., 2018. Comprehensive performance assessment of spacers in spiral-wound membrane modules accounting for compressibility effects. *J. Memb. Sci.* 549, 602–615.
- Liang, Z., Wang, J., Zhang, Y., Han, C., Ma, S., Chen, J., Li, G., An, T., 2020. Removal of volatile organic compounds (VOCs) emitted from a textile dyeing wastewater treatment plant and the attenuation of respiratory health risks using a pilot-scale biofilter. *J. Clean. Prod.* 253, 120019.
- Magdy, M., Alalm, M.G., El-Etriby, H.K., 2021. Comparative life cycle assessment of five chemical methods for removal of phenol and its transformation products. *J. Clean. Prod.* 291, 125923.
- Mohammadi, S., Kargari, A., Sanaeepour, H., Abbassian, K., Najafi, A., Mofarra, E., 2015. Phenol removal from industrial wastewaters: a short review. *Desalin. Water Treat.* 53, 2215–2234.
- Obotey Ezugbe, E., Rathilal, S., 2020. Membrane technologies in wastewater treatment: a review. *Membranes* 10 (5), 89.
- Pan, S.Y., Snyder, S.W., Packman, A.I., Lin, Y.J., Chiang, P.C., 2018. Cooling water use in thermoelectric power generation and its associated challenges for addressing water-energy nexus. *Water-Energy Nexus* 1 (1), 26–41.
- Srinivasan, G., Sundaramoorthy, S., Murthy, D.V.R., 2010. Spiral wound reverse osmosis membranes for the recovery of phenol compounds –experimental and parameter estimation studies. *Am. J. Eng. Appl. Sci.* 3 (1), 31–36.
- Sundaramoorthy, S., Srinivasan, G., Murthy, D.V.R., 2011. An analytical model for spiral wound reverse osmosis membrane modules: part I –Model development and parameter estimation. *Desalination* 280 (1–3), 403–411.
- Tortajada, C., 2020. Contributions of recycled wastewater to clean water and sanitation sustainable development goals. *NPJ Clean Water* 3 (1), 1–6.
- Zhang, X., Chen, J., Li, J., 2020. The removal of microplastics in the wastewater treatment process and their potential impact on anaerobic digestion due to pollutants association. *Chemosphere* 251, 126360.
- Zheng, C., Zhao, L., Zhou, X., Fu, Z., Li, A., 2013. Treatment technologies for organic wastewater. *Water Treat.* 11, 250–286.